Catalysis Today 147S (2009) S257–S264

Contents lists available at ScienceDirect

Catalysis Today

journal homepage: www.elsevier.com/locate/cattod

Global kinetic model for the regeneration of NO_x storage catalyst with CO, H_2 and C_3H_6 in the presence of CO_2 and H_2O

Petr Kočí [a,*], František Plát [a], Jan Štěpánek [a], Šárka Bártová [a], Miloš Marek [a], Milan Kubíček [b], Volker Schmeißer [c], Daniel Chatterjee [c], Michel Weibel [c]

[a] Department of Chemical Engineering, Center for Nonlinear Dynamics of Chemical and Biological Systems, Institute of Chemical Technology, Prague, Technická 5, CZ-166 28 Praha, Czech Republic
[b] Department of Mathematics, Center for Nonlinear Dynamics of Chemical and Biological Systems, Institute of Chemical Technology, Prague, Technická 5, CZ-166 28 Praha, Czech Republic
[c] Daimler AG, Department GR/APE – Combustion and Emission Control, 019-G206, D-70 546 Stuttgart, Germany

ARTICLE INFO

Article history:
Available online 3 August 2009

Keywords:
NO_x storage catalyst
Lean NO_x trap (LNT)
NO_x reduction selectivity
NH_3
Automobile exhaust gas conversion
Mathematical modeling

ABSTRACT

Heterogeneous 1D model with global kinetics is proposed for industrial NO_x storage and reduction catalyst (NSRC) on the basis of lab experiments in a mini-reactor in the temperature range 100–500 °C. The NO_x reduction dynamics and selectivity towards N_2 or NH_3 are modelled for three main reducing components present in the rich exhaust gas: CO, H_2, and unburned hydrocarbons (HCs). The following reactions are considered: CO, H_2 and HC oxidation, NO_x reduction, NO/NO_2 transformation, NO and NO_2 storage, oxygen storage effects, water gas shift and steam reforming, and reduction of the stored NO_x by H_2, CO and HC. Ammonia is formed mainly by the reaction of H_2 with NO_x, but also by the water-assisted reaction of CO with NO_x (formation and consequent hydrolysis of isocyanates). Inclusion of the latter route is necessary to explain the NH_3 formation in CO-rich mixtures without H_2 at lower temperatures. At higher temperatures, water gas shift and steam reforming reactions enable in situ H_2 production from CO, HC and H_2O. The formed ammonia subsequently reacts with oxygen and NO_x deposited on the catalyst surface downstream, which results in NH_3 wave travelling along the catalytic monolith.

The highest NH_3 yield is obtained around 200 °C, when the NH_3 formation from the accumulated NO_x is already ignited, while the ammonia consumption reactions are still relatively slow. At lower temperatures CO inhibits the NO_x reduction by H_2 (i.e., the NH_3 production). At higher temperatures the ammonia oxidation reactions become fast enough to eliminate most of the NH_3 produced locally from the stored NO_x. However, ammonia can be still observed after the completion of the regeneration, when it is formed steadily from the rich inlet gas containing NO_x. Model results are confronted with the lab data, and calculated evolution of concentration profiles inside the monolith is discussed. The developed model is validated by engine test driving cycle data.

1. Introduction

NO_x storage and reduction catalyst [1] (NSRC; sometimes also called lean NO_x trap, LNT) represents one of the two major technologies for catalytic elimination of NO_x emissions from diesel and lean-burn gasoline engines [2]. The alternative approach is based on selective catalytic reduction (SCR) of NO_x by NH_3 generated from urea solution [2,3].

The NSRC works in periodic lean/rich regime. During the storage phase (economical engine operation with lean fuel mixture) the NO_x are adsorbed on the catalyst surface in the form of nitrites and nitrates [4]. The accumulated NO_x are then reduced within a short rich phase (excess of reducing components CO, H_2 and HCs in the exhaust gas, lasting several seconds). Catalytic washcoat of the NSRC is usually based on γ-Al_2O_3, and contains Ce/Zr oxides as structure stabilisers with oxygen storage and low-temperature NO_x storage effects, Ba and/or other metals of I–II group as NO_x adsorbents, and noble metals as active catalytic centers for redox reactions [4–6].

Reduction of the stored NO_x can lead to different products: NO, N_2O, N_2, and NH_3. Nitrogen is usually the main product of the NO_x reduction, but the selectivity depends strongly on temperature, rich gas composition (red/ox ratio, reduction by H_2, CO and/or HCs) and the length of the regeneration phase [7,8]. Typically, NO desorption peak is emitted at the beginning of the regeneration

* Corresponding author. Tel.: +420 22044 3293; fax: +420 22044 4320.
E-mail address: petr.koci@vscht.cz (P. Kočí).
URL: http://www.vscht.cz/monolith

0920-5861/$ – see front matter © 2009 Elsevier B.V. All rights reserved.
doi:10.1016/j.cattod.2009.07.036

phase. Smaller amounts of N_2O are formed usually around the light-off temperature as the product of the incomplete NO_x reduction [8]. The ammonia outlet peak appears usually after few seconds of the regeneration, when the catalyst surface along the monolith channel is already reduced.

It has been shown that the ammonia produced at the front part of the monolith reacts with the NO_x deposited on the unreduced catalyst surface at the rear part of the monolith, which results in moving NH_3 wave along the reactor [9–12]. It was also demonstrated experimentally that ammonia itself is quite active in the NSRC regeneration [13]: when NH_3 was introduced at the reactor inlet instead of H_2, the NO_x reduction process was equivalent to the regeneration by H_2. However, this holds only for higher temperatures (i.e., mass-transport limited regeneration regime). In fact the reactivity of NH_3 is lower than that of hydrogen, and the light-off temperature of the $NO_x + H_2$ reaction is lower than that of $NO_x + NH_3$[14].

The capability to predict and control the NH_3 emissions from the NSRC is important for the application in automobiles. For the conventional NSRC configuration it is necessary to minimise the NH_3 emissions, because ammonia is an irritant gas. However, both main technologies for the NO_x abatement (NSRC and SCR) can be used together in a combined exhaust gas aftertreatment system [15]. In this two-stage NO_x reduction system the ammonia formed during the NSRC regeneration is a desired by-product, because it is adsorbed in the downstream-located SCR catalyst and utilised for the selective NO_x reduction in the next lean phase [15,16]. Design and control of such combined exhaust gas aftertreatment system can be hardly done without proper mathematical models of the individual catalysts, integrated into a common simulation environment [2].

In this paper we present a global kinetic model developed for industrial NO_x storage and reduction catalyst (NSRC) on the basis of experiments in a lab mini-reactor. We focus on the regeneration of the stored NO_x, and dynamic ammonia formation and consumption in the rich mixture containing CO, H_2 and C_3H_6. The involvement of NH_3 as a major NO_x reduction by-product and an active intermediate substantially extends our older global NSRC model [17,18], where the NO_x reduction products were represented only by N_2. The presented model is able to predict ammonia evolution during the NSRC regeneration by a complete reduction mixture (CO, H_2, HC) from low to high operating temperatures. From our results it follows that this task cannot be satisfactorily fulfilled by the NSRC models considering only H_2 as the reducing agent, or assuming H_2 as the only NH_3 source [9,12].

2. Arrangement of experiments

The lab experiments have been carried out in nearly isothermal mini-reactor, containing three identical sections of NSRC monolith (0.5 cm × 3 cm × length 2.5 cm) in series [19]. The studied catalyst was an industrial PtRh/Ba/CeO_2/ γ-Al_2O_3 washcoated on 400 cpsi cordierite monolith. Pre-treatment of the fresh catalyst samples was 1 h on stream at 500 °C with lean (oxidising) conditions, 1 h lean/rich operation at 300 °C, and 1 h lean/rich operation at 500 °C (cf. Table 1). No change of catalyst activity or storage capacity was then observed in the course of experimental series. Before each experiment, the catalyst was regenerated by the reduction using H_2-rich mixture at 400 °C to remove the adsorbed NO_x.

The inlet mixture was prepared from synthetic gases (CO, O_2, C_3H_6, H_2, NO, NO_2, CO_2, H_2O, and N_2) using on-line mass flow controllers with transient response time $\leq$ 1 s. Periodic lean/rich (300 s/20 s) operation was examined in the temperature range 100–500 °C with $\Delta T = 50$ K. At low temperatures the NSRC regeneration is often incomplete and it takes several periods before the operation stabilises [9,17]. Therefore, eight lean + rich periods were performed at each temperature and the last one was considered as the stabilised one. Although very small monolith sections (three channels thick slices) were used, the lean/rich operation was still not completely isothermal due to heat evolution during the rich phase. The maximum observed temperature increase (at higher temperatures) was approximately 20 K and this was considered in the simulations. Three reducing agents (H_2, CO and C_3H_6) were tested individually, and additionally the mixture of H_2 with CO was tested to check the inhibition effect of CO on the H_2 reactions. The composition of the inlet gas is given in Tables 1 and 2.

Table 1
Conditions in the lean (storage) and rich (regeneration) phase used in lab experiments and simulations. Inlet gas composition is given in mole fractions.

Variable	Lean phase (storage)	Rich phase (regeneration)
τ	300 s	20 s
GHSV	30 000 h^{-1}	30 000 h^{-1}
T^{in}	100–500 °C	100–500 °C
y^{in}_{NO}	500 ppm	500 ppm
$y^{in}_{NO_2}$	0 ppm	0 ppm
$y^{in}_{O_2}$	7%	0.2%
$y^{in}_{H_2}$	0%	cf. Table 2
y^{in}_{CO}	0%	cf. Table 2
$y^{in}_{C_3H_6}$	0 ppm	cf. Table 2
$y^{in}_{NH_3}$	0 ppm	0 ppm
$y^{in}_{CO_2}$	5%	5%
$y^{in}_{H_2O}$	5%	5%
$y^{in}_{N_2}$	Balance	Balance

The outlet concentrations were sampled by IR absorption analyser (ABB Advanced Optima Uras—CO and CO_2; $\Delta t = 1$ s), UV absorption analyser (ABB Advanced Optima Limas—NO, NO_2 and NH_3; $\Delta t = 1$ s), and mass spectrometer (Pfeiffer Vacuum Omnistar GSD301—O_2, HC and H_2; $\Delta t = 0.5$ s). The sampling lines were heated to 180 °C to minimise adsorption or condensation.

3. Mathematical model

Standard, spatially pseudo-1D, heterogeneous model of monolith channel with plug flow and surface deposition of gas components is employed in the simulations [2,17]. Unlike the 2D(1D + 1D) model with explicit solution of diffusion effects in the washcoat [2,20,21] or even more detailed 3D models of washcoat structure [22], the internal diffusion effects in the used heterogeneous 1D model are lumped into effective reaction rate parameters for given washcoat structure, i.e., the effective kinetic parameters need to be adjusted for each new catalyst formulation (though the modifications are often mild). This is a commonly accepted trade-off enabling simulations with short computation times even for complex reaction systems, which is desired for practical application in automobile industry [2]. It is well known that the NSRC reaction kinetics is inherently influenced by local transport on the catalytic surface (size, proximity and mutual contact of noble metal sites, NO_x storage material and oxygen storage components) and usually more than one kind of NO_x adsorbent is present in the washcoat. In such a complicated

Table 2
Tested rich gas mixtures, composition in mole fractions.

Rich mixture	H_2	CO	H_2+CO	C_3H_6
$y^{in}_{H_2}$	3.3%	0%	2.3%	0%
y^{in}_{CO}	0%	3.3%	1.0%	0%
$y^{in}_{C_3H_6}$	0 ppm	0 ppm	0 ppm	3667 ppm

Note: All rich mixtures are equivalent with respect to the redox reactions stoichiometry; the propylene concentration 3667 ppm corresponds to 3.3% CO or H_2.

Table 3
Global reaction kinetic model for NO_x storage and reduction catalyst (NSRC), including NH_3 formation and consumption reactions.

Reaction step	Reaction rate
$CO + \frac{1}{2}O_2 \rightarrow CO_2$	$R_1 = k_1 A_{NM} y_{CO} y_{O_2}/G_1$
$H_2 + \frac{1}{2}O_2 \rightarrow H_2O$	$R_2 = k_2 A_{NM} y_{H_2} y_{O_2}/G_1$
$C_3H_6 + \frac{9}{2}O_2 \rightarrow 3CO_2 + 3\,H_2O$	$R_3 = k_3 A_{NM} y_{C_3H_6} y_{O_2}/G_1$
$H_2O + CO \rightleftharpoons CO_2 + H_2$	$R_4 = k_4 A_{NM} [y_{CO} y_{H_2O} - y_{CO_2} y_{H_2}/K^{eq}_{y,4}]$
$3\,H_2O + C_3H_6 \rightarrow 3CO + 6\,H_2$	$R_5 = k_5 A_{NM} [y_{C_3H_6} y_{H_2O} - y^3_{CO} y^6_{H_2}/(K^{eq}_{y,5} y^2_{H_2O})]$
$NO + CO \rightarrow CO_2 + \frac{1}{2}N_2$	$R_6 = k_6 A_{NM} y_{CO} y^{0.5}_{NO}/G_1/G_2$
$NO + \frac{5}{2}H_2 \rightarrow H_2O + NH_3$	$R_7 = k_7 A_{NM} y_{H_2} y^{0.5}_{NO}/G_1/G_2$
$9NO + C_3H_6 \rightarrow 3CO_2 + 3\,H_2O + \frac{9}{2}N_2$	$R_8 = k_8 A_{NM} y_{C_3H_6} y^{0.5}_{NO}/G_1/G_2$
$NO + \frac{1}{2}O_2 \rightleftharpoons NO_2$	$R_9 = k_9 A_{NM} [y_{NO} y^{0.5}_{O_2} - y_{NO_2}/K^{eq}_{y,9}]/G_1$
$Ce_2O_3 + \frac{1}{2}O_2 \rightarrow Ce_2O_4$	$R_{10} = k_{10} A_{NM} \Psi_{cap,O_2} y_{O_2} (\psi^{eq}_{O_2} - \psi_{O_2})$
$Ce_2O_4 + CO \rightarrow Ce_2O_3 + CO_2$	$R_{11} = k_{11} A_{NM} \Psi_{cap,O_2} y_{CO} \psi_{O_2}$
$Ce_2O_4 + H_2 \rightarrow Ce_2O_3 + H_2O$	$R_{12} = k_{12} A_{NM} \Psi_{cap,O_2} y_{H_2} \psi_{O_2}$
$Ce_2O_4 + \frac{1}{9}C_3H_6 \rightarrow Ce_2O_3 + \frac{1}{3}CO_2 + \frac{1}{3}H_2O$	$R_{13} = k_{13} A_{NM} \Psi_{cap,O_2} y_{C_3H_6} \psi_{O_2}$
$2NO_2 + \frac{1}{2}O_2 + BaCO_3 \rightarrow Ba(NO_3)_2 + CO_2$	$R_{14} = k_{14} A_{NM} \Psi_{cap,NO_x} y_{NO_2} (\psi^{eq}_{NO_x} - \psi_{NO_x})^2$
$2\,NO + \frac{3}{2}O_2 + BaCO_3 \rightleftharpoons Ba(NO_3)_2 + CO_2$	$R_{15} = k_{15} A_{NM} \Psi_{cap,NO_x} y_{NO} (\psi^{eq}_{NO_x} - \psi_{NO_x})^2$
$Ba(NO_3)_2 + 5\,CO \rightarrow BaO + 5\,CO_2 + N_2$	$R_{16} = k_{16} A_{NM} \Psi_{cap,\,NO_x} y_{CO} \psi^2_{NO_x}/G_3$
$Ba(NO_3)_2 + 8\,CO + 3\,H_2O \rightarrow BaO + 8\,CO_2 + 2NH_3$	$R_{17} = k_{17} A_{NM} \Psi_{cap,NO_x} y_{CO} \psi^2_{NO_x}/G_3/G_5$
$Ba(NO_3)_2 + 8\,H_2 \rightarrow BaO + 5\,H_2O + 2\,NH_3$	$R_{18} = k_{18} A_{NM} \Psi_{cap,NO_x} y_{H_2} \psi^2_{NO_x}/G_3/G_5$
$Ba(NO_3)_2 + \frac{5}{9}C_3H_6 \rightarrow BaO + \frac{5}{3}CO_2 + \frac{5}{3}H_2O + N_2$	$R_{19} = k_{19} A_{NM} \Psi_{cap,NO_x} y_{C_3H_6} \psi^2_{NO_x}/G_3$
$Ba(NO_3)_2 + 3\,CO \rightarrow BaO + 3\,CO_2 + 2\,NO$	$R_{20} = k_{20} A_{NM} \Psi_{cap,\,NO_x} y_{CO} \psi^2_{NO_x}/G_4$
$Ba(NO_3)_2 + 3H_2 \rightarrow BaO + 3\,H_2O + 2\,NO$	$R_{21} = k_{21} A_{NM} \Psi_{cap,\,NO_x} y_{H_2} \psi^2_{NO_x}/G_4$
$Ba(NO_3)_2 + \frac{1}{3}C_3H_6 \rightarrow BaO + CO_2 + H_2O + 2\,NO$	$R_{22} = k_{22} A_{NM} \Psi_{cap,\,NO_x} y_{C_3H_6} \psi^2_{NO_x}/G_4$
$\frac{10}{3}NH_3 + Ba(NO_3)_2 \rightarrow BaO + 3\,H_2O + \frac{8}{3}N_2$	$R_{23} = k_{23} A_{NM} \Psi_{cap,NO_x} y_{NH_3} \psi^2_{NO_x}$
$2\,NH_3 + 3\,NO \rightarrow \frac{5}{2}N_2 + 3\,H_2O$	$R_{24} = k_{24} A_{NM} y_{NH_3} y^{0.5}_{NO}$
$2\,NH_3 + \frac{3}{2}O_2 \rightarrow N_2 + 3\,H_2O$	$R_{25} = k_{25} A_{NM} y_{NH_3} y_{O_2}$
$2\,NH_3 + 3\,Ce_2O_4 \rightarrow N_2 + 3\,H_2O + 3\,Ce_2O_3$	$R_{26} = k_{26} A_{NM} \Psi_{cap,O_2} y_{NH_3} \psi_{O_2}$
$BaO + CO_2 \rightarrow BaCO_3$	$R_{27} = \sum_{j=16}^{23} R_j$

$G_1 = (1 + K_{a,1} y_{CO} + K_{a,2} y_{C_3H_6})^2 \cdot (1 + K_{a,3} y^2_{CO} y^2_{C_3H_6}) \cdot (1 + K_{a,4} y^{0.7}_{NO_x})\, T^s$; $G_2 = 1 + K_{a,5} y_{O_2}$; $G_3 = 1 + K_{a,6} y_{O_2}$; $G_4 = (1 + 0.1\,K_{a,6} y_{O_2}) \cdot (1 + K_{a,7} y_{NO_x})$; $G_5 = 1 + K_{a,8} y_{CO}$. From historical reasons the form of G_1 is taken after classical work [27].

situation virtually any mean-field reaction kinetic model implicitly includes at least part of the internal transport effects.

The following balances are considered in the model [2,17]: (i) component mass balances in the flowing gas, including accumulation, convection, and external mass transfer; (ii) component mass balances in the washcoat pores (gas), including accumulation, external mass transfer, and catalytic reactions; (iii) component mass balances on the catalyst surface, including accumulation, adsorption/desorption and catalytic reactions; (iv) enthalpy balance of the flowing gas, including accumulation, convection, and gas–solid heat transfer; and (v) enthalpy balance of the solid phase, including accumulation, axial heat conduction, gas–solid heat transfer, and heat source from catalytic reactions.

The model has been coded in Fortran as a part of the versatile software package for dynamic simulations of interconnected systems of catalytic reactors and adsorbers, developed at the Institute of Chemical Technology, Prague [6,9,19,17,20–23].

4. Reaction scheme

The proposed NSRC model reactions and global rate laws are listed in Table 3. Just two adsorbed components with major accumulation effects are considered explicitly on the surface (ψ_{NO_x} and ψ_{O_2}). Their storage phenomena are characterised by the maximum storage capacities Ψ^{cap}_m, temperature dependences of the saturation coverages $\psi^{eq}_m(T)$, and global rate coefficients $k_j(T)$ [6,17]. As the H_2O and CO_2 are always present in the exhaust gas in relative excess, their effects on the NO_x and O_2 storage are implicitly included in the parameters. The catalytic activity of noble metals (proportional to their loading and dispersion) is represented by the coefficient A_{NM}.

In comparison with more detailed NSRC micro-kinetic models (e.g. [12]), this approach leads to a lower number of reaction steps and species to be balanced, and to a lower stiffness of the system for numerical solution. The resulting model then enables simulations under realistic conditions (complex exhaust gas mixture) with comfortable computation times, while it still keeps essential reliability and robustness [2,18].

The presented reaction scheme in Table 3 extends the basic NSRC model developed earlier [17,18], where N_2 was considered as the only product of the NO_x reduction. The sub-model for the reactions of hydrogen with NO_x leading to ammonia was discussed already in [9]. Even if hydrogen is very active reducing agent, its concentration in real exhaust gas is not dominant—in a realistic model high CO and HC concentrations need to be considered concurrently in the rich mixture. In this paper we propose such global NSRC kinetic model, considering the NH_3 formation and consumption reactions in the case of the regeneration by CO, H_2 and C_3H_6 with mutual inhibition effects, and including reactions with water.

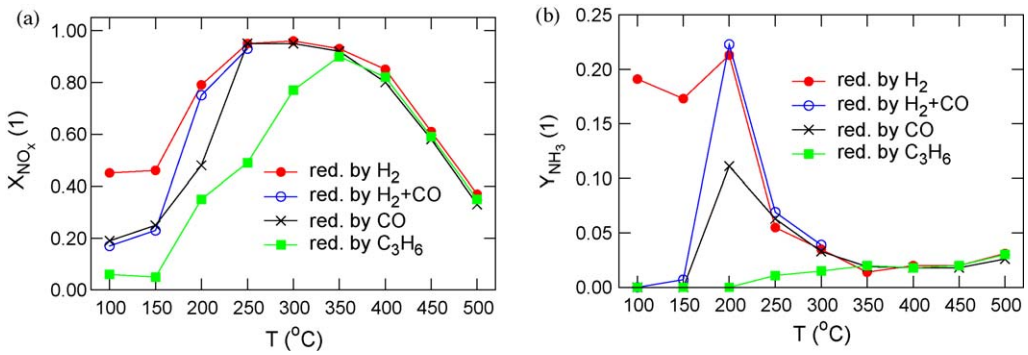

Fig. 1. Temperature dependence of integral NO_x conversion X_{NO_x} and integral ammonia yield Y_{NH_3} during periodic lean/rich operation with different reducing mixtures (cf. Tables 1 and 2). Lab reactor, GHSV = 30 000 h^{-1}, $\tau^{lean} = 300$ s, $\tau^{rich} = 20$ s.

The following reactions are involved (cf. Table 3): CO, H_2 and HC oxidation (R_1–R_3), water gas shift and steam reforming (R_4–R_5), NO_x reduction (R_6–R_8), NO/NO_2 transformation (R_9), oxygen storage effects (R_{10}–R_{13}), NO and NO_2 storage (R_{14}–R_{15}), "direct" reduction of the stored NO_x by H_2, CO and HC (spill-over to noble metal sites without NO desorption to gas phase; R_{16}–R_{19}), desorptive decomposition of the stored NO_x (R_{20}–R_{22}), and ammonia oxidation via reactions with the NO_x and oxygen (R_{23}–R_{26}). The N_2O (by-product of the NO_x reduction observed in minor concentrations at lower temperatures) is neglected in this approximation. Based on experimental observations, it is further assumed that under rich conditions the reactions $NO_x + H_2$ lead to NH_3 (R_7, R_{18}), while formation of both N_2 and NH_3 is possible for NO_x + CO reaction (R_6, R_{16}, R_{17}). For the NO_x reduction by C_3H_6, nitrogen is the only product considered (R_8, R_{19}). Kinetic parameters for the reactions R_1–R_{15} were adopted from the older model [17,18], just the inhibition of the NO_x reduction was extended (R_6–R_8). The steady state NO_x, CO, H_2 and HC conversions were examined by the light-off experiments with slow temperature ramps. Several lean and rich mixtures were tested and the model is able to predict the steady-state conversions correctly.

The NSRC regeneration parameters including NH_3 reactions were newly evaluated from the lab experiments by simplex optimisation method, using the weighted sum of squares of the differences between the simulated and measured outlet concentrations of key gas components as the objective function. In the next section, the proposed reaction scheme is discussed in more detail and confronted with experimental data.

5. Results

Integral characteristics of the (stabilised) periodic lean + rich operation evaluated from the series of lab experiments are summarised in Fig. 1. The following trends in NO_x conversion can be seen in Fig. 1a: (i) the activity of the NO_x reduction decreases in the order $H_2 > CO > C_3H_6$, with outstandingly low activity of propylene; (ii) the high activity of H_2 at temperatures 100–150 °C is significantly inhibited by CO present in the rich mixture; (iii) the highest NO_x conversion is obtained at 250–300 °C for the reduction by CO and H_2, and at 350 °C for C_3H_6; (iv) at the temperatures above 350 °C the NO_x conversion is independent of the used reducing agent. These results indicate that at lower temperatures the regeneration is kinetically limited, while at higher temperatures it is controlled by mass transport. Decrease of the NO_x conversion at high temperatures is caused by the thermodynamically driven loss of effective NO_x adsorption capacity $\psi^{eq}_{NO_x}(T)$ [5,6,9].

The highest ammonia yield (Fig. 1b) is obtained by the NSRC regeneration with H_2 and H_2+CO mixtures at 200 °C. At lower temperatures 100–150 °C the NH_3 yield with pure H_2 is still quite high. In fact, the integral selectivity of $NO_x + H_2$ towards NH_3 even increases with the decreasing temperature (cf. [9])—the lower NH_3 yield at 100–150 °C is caused by the lower overall NO_x conversion.

In contrast to the regeneration by pure H_2, the ammonia yield drops to zero at 100–150 °C in the case of the H_2+CO rich mixture. This indicates significant inhibition of the NO_x+H_2 reactions leading to NH_3 (R_7 and R_{18} in Table 3). Because the real exhaust gas always contains CO even in higher concentrations than H_2, it is quite important to consider this inhibition effect in the model (cf. G_1 and G_5 in Table 3). At the temperatures above 250 °C the ammonia yield decreases due to the acceleration of ammonia oxidation [14], cf. reactions R_{23}–R_{26} in Table 3.

During the development of the model we started with the hypothesis that the NH_3 formation in the case of the NO_x reduction by CO in the presence of water proceeds primarily via water gas shift reaction, forming hydrogen [9]. However, the analysis of the experimental data and simulations revealed that significant amounts of NH_3 are formed during the NSRC regeneration by CO already below the water gas shift light-off temperature, which also is in agreement with the observations [24]. It can be seen in Fig. 2a that almost no H_2 is produced below 250 °C, while quite high NH_3 yield is obtained during the NSRC regeneration by CO already at 200 °C. Thus, the "direct" water-assisted reduction of NO_x by CO up to NH_3 (proceeding most probably via formation and consequent hydrolysis of isocyanates [25,26]) is necessary for correct description of NH_3 formation with CO-rich mixtures at lower temperatures (cf. R_{17} in Table 3). Concurrently, the "standard" NO_x reduction by CO leading to N_2 still need to be considered—cf. the approximately 25% NO_x conversion without significant NH_3 formation at 150 °C in Fig. 1. Only very small amounts of NH_3 were detected in the case of the NSRC regeneration by C_3H_6 below the light-off of the steam reforming reaction (compare Figs. 2b and 1b). Therefore, in our model the NO_x reduction by C_3H_6 itself is considered to produce N_2 (R_8 and R_{19} in Table 3).

Dynamic evolution of the NO_x and NH_3 concentrations in the course of the stabilised periodic lean/rich operation at 150 °C is shown in Fig. 3. In all cases the time $t = 0$ s corresponds to the start of the regeneration phase where the NO_x desorption, NO_x reduction, and NH_3 formation take place. At the time $t = 20$ s the lean mixture is introduced and the NO_x adsorption occurs. Gradual saturation of the catalyst storage capacity result in the increasing trend of the outlet NO_x concentration during the lean phase. The situation when the outlet NO_x concentration reaches the inlet NO_x level corresponds to the fully saturated storage capacity. At the time $t = 320$ s the next regeneration phase is applied and the process is periodically repeated. At this lower temperature the regeneration process is kinetically limited and the

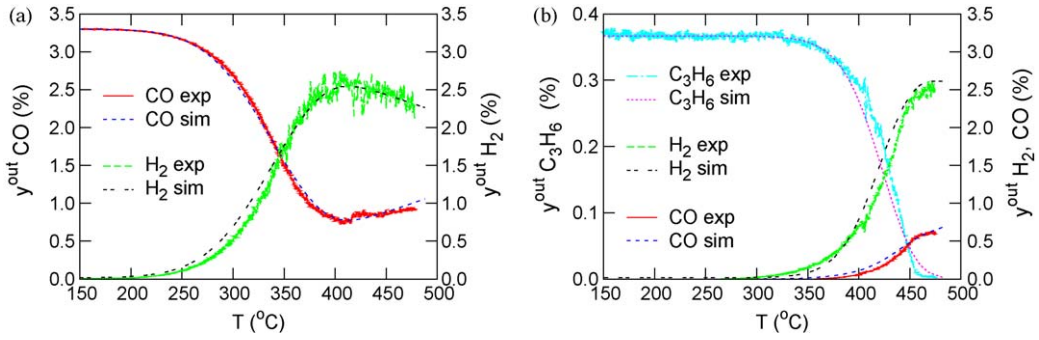

Fig. 2. Activity of reactions producing hydrogen under rich conditions: (a) water gas shift ($y^{in}_{CO} = 3.3\%$), (b) steam reforming ($y^{in}_{C_3H_6} = 0.37\%$). Lab reactor, slow temperature ramp 3 K min^{-1}, $y^{in}_{CO_2} = 5\%$, $y^{in}_{H_2O} = 5\%$, $y^{in}_{O_2} = 0$ ppm, $y^{in}_{NO_x} = 0$ ppm, GHSV = 30 000 h^{-1}.

regeneration of the stored NO_x is not complete, so that the differences between the individual rich mixtures can be clearly seen. Higher outlet NO_x concentrations during the lean (adsorption) phase indicate smaller extent of the regeneration. The rich mixture containing only hydrogen (Fig. 3a) is already quite effective, giving only small NO_x desorption peak and relatively high NO_x conversion, but also large ammonia peak almost immediately after the start of the regeneration. This is caused by already high activity of the NO_x+H_2 reactions (NH_3 formation), and very slow NH_3+NO_x and NH_3+O_2 reactions (NH_3 consumption) at this low temperature.

It must be noted here that the used analysers are not able to capture exactly the sharp maxima of the NO_x and NH_3 peaks due to relatively large inner volumes of the measurement cells, leading to dispersion of the signals. Thus the integrals of the peaks (i.e., total NO_x and NH_3 amounts emitted) are considered in the evaluation rather than the exact values of the maxima.

In the case of the H_2+CO rich mixture (Fig. 3b) the regeneration is inhibited by the presence of CO—higher NO_x desorption peak, lower overall NO_x conversion, and much lower NH_3 peak are obtained (note the scales of the y_{NH_3} axes). The CO inhibition effect at 150 °C is so strong that the results with the H_2+CO rich mixture are very similar to the results obtained with pure CO (Fig. 3c). Here only very small amounts of NH_3 are produced. Almost no activity of propylene at this low temperature is demonstrated in Fig. 3d.

As discussed earlier (Figs. 1b and 2a), significant NH_3 formation during the NSRC regeneration by CO can be seen already at 200 °C, below the light-off of the water gas shift reaction. This is demonstrated in Fig. 4. Both NO_x storage and regeneration processes are more effective at 200 °C than at 150 °C, resulting in significantly higher integral NO_x conversion. The NH_3 oxidation rates also increase with temperature—this is reflected in slight delay of the outlet NH_3 peak in Fig. 4. However, the NH_3 + NO_x recombination is still relatively slow at 200 °C so that the high NH_3 yield is obtained.

Comparison of the periodic lean/rich operation with the CO and C_3H_6 rich mixtures at 250 °C is given in Fig. 5. At this temperature the effectivity of the regeneration by CO practically reaches that of H_2 (cf. Fig. 1), but the C_3H_6 is still significantly less active reducing agent. In the case of CO (Fig. 5a) we can observe an excellent NO_x

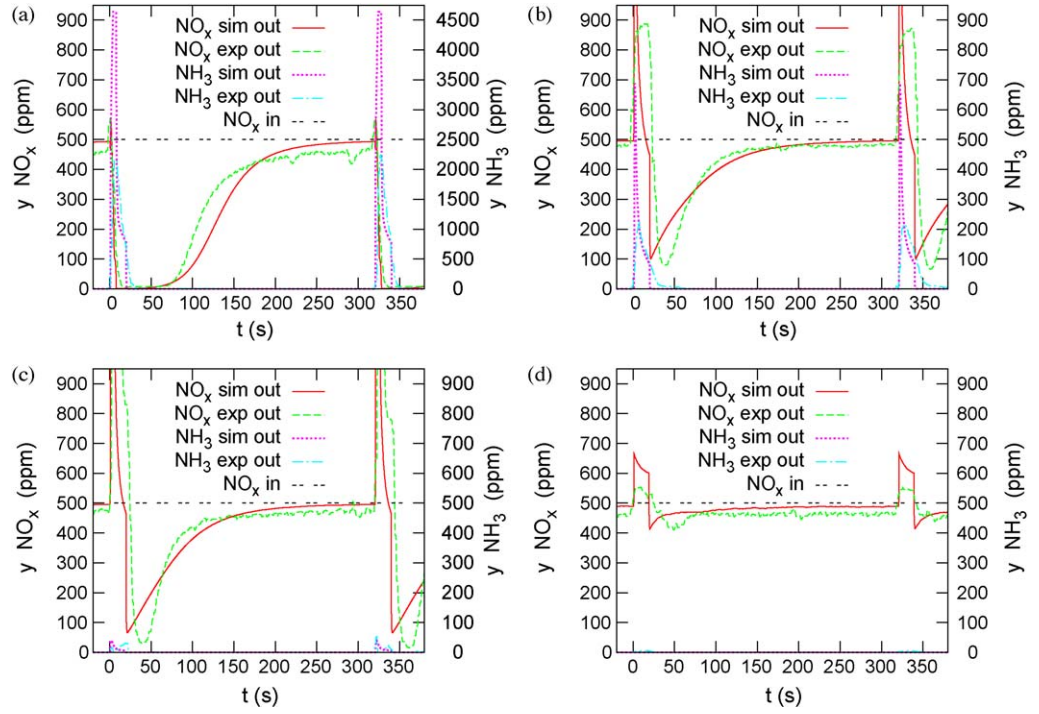

Fig. 3. Outlet NO_x and NH_3 concentrations during periodic lean/rich operation with different reducing mixtures at 150 °C. Lab reactor, GHSV = 30 000 h^{-1}, $\tau^{lean} = 300$ s, $\tau^{rich} = 20$ s. (a) H_2-rich mixture, (b) H_2+CO rich mixture, (c) CO-rich mixture and (d) C_3H_6-rich mixture (cf. Tables 1 and 2).

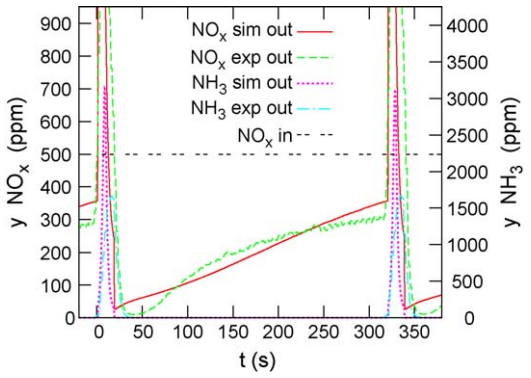

Fig. 4. Outlet NO_x and NH_3 concentrations during periodic lean/rich operation with CO-rich mixture at 200 °C. Lab reactor, GHSV = 30 000 h^{-1}, $\tau^{lean} = 300$ s, $\tau^{rich} = 20$ s, cf. Tables 1 and 2.

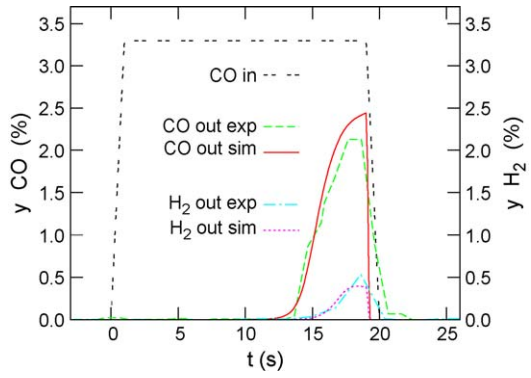

Fig. 6. Outlet CO and H_2 concentrations during rich phase of periodic lean/rich operation at 250 °C. Lab reactor, GHSV = 30 000 h^{-1}, $\tau^{lean} = 300$ s, $\tau^{rich} = 20$ s, CO rich mixture (cf. Tables 1 and 2).

conversion, with the outlet NH_3 peak delayed several seconds after the start of the regeneration. This delay indicates that the NH_3 recombination reactions are already quite active at 250 °C—during the initial stage of the regeneration the NH_3 produced locally in the front part of the monolith is effectively eliminated in the still oxidised rear part [9]. In the case of C_3H_6 (Fig. 5b) the NO_x conversion is lower, with quite high NO_x desorption peak, and almost no NH_3 is produced.

Detail of the outlet CO and H_2 concentrations in the course of the NSRC regeneration by CO at 250 °C is shown in Fig. 6. It can be seen that hydrogen is produced from CO under rich conditions, and both CO and H_2 appear at the reactor outlet with significant delay that is determined by the speed of the regeneration front from the reactor inlet to the outlet. Until the CO and H_2 breakthrough all the reducing agents are consumed by the reactions with the NO_x and oxygen accumulated in the reactor after the preceding lean phase. As the NH_3 also belongs to active reducing agents, it appears at the outlet with similar delay as the CO and H_2 (compare Figs. 5a and 6).

Outlet NO_x and NH_3 concentrations in the course of the lean + rich period with C_3H_6 rich mixture at 370 °C are shown in Fig. 7a. At this temperature the steam reforming reaction becomes active (cf. Fig. 2b) and the H_2 and CO are produced in situ from C_3H_6. This results in similar NO_x conversions and NH_3 yields for all the reducing mixtures (cf. Fig. 1). The ammonia peak at 370 °C is significantly delayed, quite narrow, and smaller than observed at lower temperatures. This is caused by fast NH_3 oxidation reactions that eliminate most of the ammonia produced locally from the adsorbed NO_x. At even higher temperatures ($\geq$450 °C) the net NH_3 yield from the pre-adsorbed NO_x is negligible. Under such conditions the ammonia is obtained only after the completion of the catalyst surface reduction, and the main NH_3 source is then steady reduction of the NO_x contained in the rich inlet gas.

Concentration profile of key components inside the NSRC monolith in the middle of the regeneration phase with C_3H_6 at 370 °C is depicted in Fig. 7b. At the end of the lean phase the NO_x are stored mostly in the front part of the monolith (cf. "NO_x surf. init." in Fig. 7b), as the NO_x adsorption front proceeded slowly from the reactor inlet to the outlet (the regeneration starts before the complete NO_x breakthrough). The reduction front (located on the boundary between reduced and oxidised part) is travelling along the monolith channel towards the reactor outlet [9]. The speed of the front movement is not constant, it depends on the local coverage of the stored NO_x and oxygen—the higher initial NO_x coverage at the front part of the monolith results in a slower movement of the reduction front (higher amount of the reducing agents is consumed for the reduction of the catalyst surface), while the lower initial NO_x coverage speeds-up the reduction front in the rear part of the monolith [9]. Furthermore, higher amount of the primary reducing agents (CO, H_2, C_3H_6) is consumed during the initial stage of the surface NO_x reduction up to NH_3, when the internal NH_3 peak is being established. Later, when the NH_3 wave moves through the reactor, the overall NH_3 formation and NH_3 oxidation rates are nearly balanced, so that the consumption of the primary reducing agents per reduced NO_x mole decreases.

At this higher temperature, steam reforming and water gas shift take place inside the reduced part of the monolith. This is reflected in gradually increasing H_2 and CO concentrations in the front part of the reactor (cf. Fig. 7b). At the boundary between the reduced and the oxidised (rear) part of the monolith, the H_2 and CO concentrations start to decrease again as they are consumed by the reactions with the stored NO_x and oxygen.

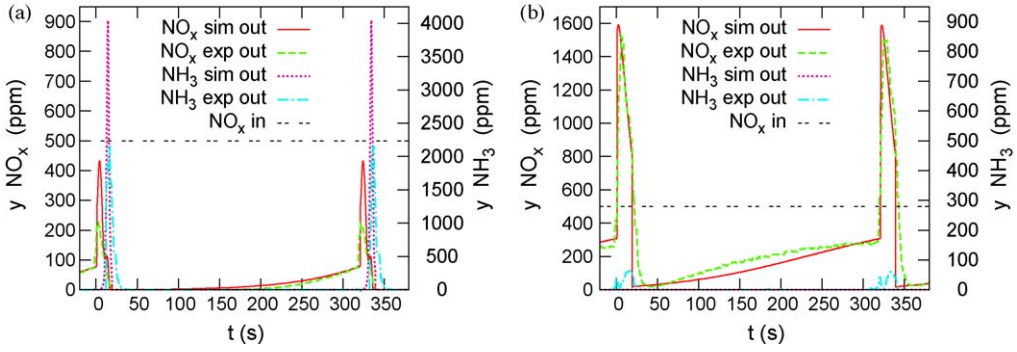

Fig. 5. Outlet NO_x and NH_3 concentrations during periodic lean/rich operation with different reducing mixtures at 250 °C. Lab reactor, GHSV = 30 000 h^{-1}, $\tau^{lean} = 300$ s, $\tau^{rich} = 20$ s. (a) CO-rich mixture and (b) C_3H_6-rich mixture (cf. Tables 1 and 2).

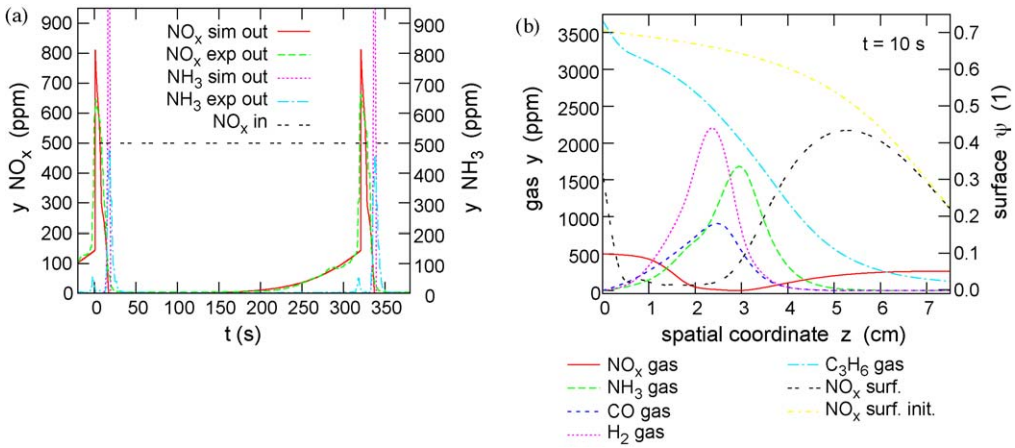

Fig. 7. Periodic lean/rich operation with C_3H_6-rich mixture at 370 °C. (a) Outlet NO_x and NH_3 concentrations and (b) calculated concentration profiles inside the monolith reactor in the middle of the regeneration. Lab reactor, GHSV = 30 000 h^{-1}, $\tau^{lean} = 300$ s, $\tau^{rich} = 20$ s, cf. Tables 1 and 2.

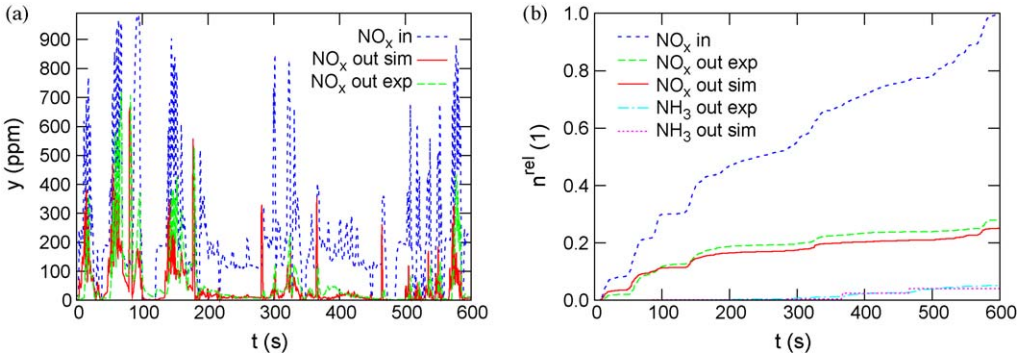

Fig. 8. NO_x and NH_3 emissions during engine test driving cycle SFTP-US06. (a) Dynamic evolution of NO_x molar fractions y and (b) normalised cumulative NO_x and NH_3 emissions n^{rel}. Full-size adiabatic NSRC monolith, GHSV = 5000–400 000 h^{-1} (average GHSV = 55 000 h^{-1}).

The gas NO_x concentration in the reduced zone decreases to zero due to the NO_x reduction by C_3H_6, H_2 and CO. However, the reaction of the reducing agents with the spare oxygen in the rich inlet gas is preferred (cf. the steeper initial decrease of the C_3H_6 concentration near the inlet). The NO_x are considerably reduced only after the depletion of the spare oxygen—this results in a small NO_x plateau in the inlet region. After the reduction of the NO_x from the inlet gas, the NO_x concentration increases again on the redox boundary due to the desorption of the stored NO_x.

Ammonia is formed in two stages by the reactions of NO_x with H_2 and CO + H_2O (Fig. 7b): The first stage occurs close to the inlet, where the NO_x from the inlet gas are reduced. The second stage takes place at the moving boundary between the reduced and the oxidised part of the monolith, where the stored NO_x are reduced. After reaching the oxidised zone, the ammonia concentration decreases again as it reacts with the stored oxygen and NO_x. When the reducing front reaches the reactor outlet, the ammonia peak is observed in the exhaust (together with the breakthrough of other reducing agents). Evolution of the reduction front is most pronounced at higher temperatures. With the decreasing temperature the reactions become slower, which results in milder internal concentrations gradients and wider boundary zone between the reduced and the oxidised part of the monolith.

After the model was fitted to the lab data, the SFTP-US06 [3] driving cycle data from passenger car dynamometer measurements with full-size monolith were used for the model validation. The SFTP-US06 standard driving cycle represents aggressive, high acceleration driving behaviour with rapid speed fluctuations [3]. The average GHSV was 55 000 h^{-1}, with maxima approximately 400 000 h^{-1}. The evolution of instantaneous NO_x concentrations in the course of the driving cycle is given in Fig. 8a. The corresponding NO_x and NH_3 cumulative emissions are depicted in Fig. 8b—they include the effect of fluctuating flow-rate. All the cumulative emissions are normalised by the integrated inlet (raw) NO_x emissions over the complete test cycle. The regeneration phases are indicated by the outlet NO desorption peaks in Fig. 8a and/or increase of cumulative outlet NH_3 emissions in Fig. 8b. The model predictions agree well with the measurements. During this validation all the kinetic parameters were kept constant except the maximum NO_x storage capacity $\Psi^{eq}_{NO_x}$ that was approximately 15% lower due to partial ageing of the catalyst caused by the operation with sulfur-containing fuel.

6. Conclusions

Effective global kinetic model has been developed for simulations of the real NSRC converter operation with periodic alternation of longer lean and short rich phase. The catalyst regeneration by CO, H_2 and HC in the presence of CO_2 and H_2O is considered. Dynamics of the stored NO_x reduction and selectivity towards N_2/NH_3 was examined by lab experiments in the temperature range 100–500 °C and the global reaction scheme has been proposed. The following aspects influencing the NO_x conversion and NH_3 selectivity are considered in the model:

- The activity of the NO_x reducing agents is $H_2 > CO > C_3H_6$.

- Ammonia is formed mainly by the reaction of H_2 with NO_x, as well as by the water-assisted reaction of CO with NO_x (formation and consequent hydrolysis of isocyanates). The latter route is necessary to explain the NH_3 formation in CO-rich mixtures without H_2 at lower temperatures, below the light-off of water gas shift.
- CO significantly inhibits the NO_x reduction by H_2, and NH_3 production at low temperatures.
- At higher temperatures, water gas shift and steam reforming enable in situ H_2 production from CO, HC and H_2O, and all the reducing agents become equivalent for the regeneration.
- The formed ammonia can react with oxygen and NO_x deposited on the catalyst surface downstream, which results in an NH_3 wave travelling along the monolith during the regeneration phase. When the wave reaches the reactor outlet, ammonia peak is observed in the outlet gas.
- The highest NH_3 yield is obtained at intermediate temperatures (around 200 °C), when the NH_3 formation from the accumulated NO_x is already ignited, while the ammonia consumption reactions are still relatively slow.
- At high temperatures the ammonia oxidation reactions become fast enough to eliminate most of the NH_3 produced locally from the stored NO_x. However, ammonia can be still formed after the completion of the regeneration from the rich inlet gas containing NO_x.
- Oxygen storage effects influence the balance of the reducing agents in the regeneration phase.
- The increased NH_3 selectivity typically observed for an aged NSRC can be well described by the presented model. Among others, consideration of lower values of the NH_3 oxidation rate coefficients (k_{23}–k_{26} in Table 3) leads to higher net NH_3 emissions at lower and intermediate temperatures. Another aspect influences the NH_3 yield at higher temperatures: the lower overall NO_x storage capacity Ψ_{cap,NO_x} of the aged catalyst leads to earlier breakthrough of the NH_3 wave.

The developed model forms a useful tool for prediction and control of the NH_3 emissions from the NSRC. It was validated by engine test driving cycle data and integrated into a common environment used for simulations of combined exhaust gas aftertreatment systems [2]. Different operating conditions and regeneration strategies can be chosen in dependence on desired NO_x reduction selectivity determined by actual configuration of exhaust gas aftertreatment system. For conventional NSRC application the NH_3 formation should be avoided, while for the combined NSRC + SCR systems ammonia is a desired functional by-product utilised in the SCR catalyst [15,16].

Acknowledgements

The work was supported by the project MSM 6046137306 (Czech Ministry of Education) and the grant GACR 104/08/1162 (Czech Grant Agency). Norbert Waldbüßer (Daimler AG) is acknowledged for measuring the test driving cycle data.

References

[1] N. Takahashi, H. Shinjoh, T. Iijima, T. Suzuki, K. Yamazaki, K. Yokota, H. Suzuki, N. Miyoshi, S. Matsumoto, T. Tanizawa, T. Tanaka, S. Tateishi, K. Kasahara, Catal. Today 27 (1996) 63.
[2] A. Güthenke, D. Chatterjee, M. Weibel, B. Krutzsch, P. Kočí, M. Marek, I. Nova, E. Tronconi, Current status of modelling lean exhaust gas aftertreatment catalysts, in: G.B. Marin (Ed.), Adv. Chem. Eng., vol. 33, Elsevier, Amsterdam, 2007, pp. 103–211.
[3] DieselNet, Diesel emissions online, http://www.dieselnet.com (2009).
[4] W.S. Epling, L.E. Campbell, A. Yezerets, N.W. Currier, J.E. Parks, Catal. Rev. 46 (2004) 163.
[5] T. Kobayashi, T. Yamada, K. Kayano, SAE Tech. Paper 970745 (1997).
[6] P. Kočí, M. Kubíček, M. Marek, T. Maunula, M. Härkönen, Chem. Eng. J. 97 (2004) 131.
[7] J.A. Pihl, J.E. Parks II, C.S. Daw, T.W. Root, SAE Tech. Paper 2006-01-3441 (2006).
[8] W.S. Epling, A. Yezerets, N.W. Currier, Appl. Catal. B: Environ. 74 (2007) 117.
[9] P. Kočí, F. Plát, J. Štěpánek, M. Kubíček, M. Marek, Catal. Today 137 (2008) 253.
[10] S.S. Mulla, S.S. Chaugule, A. Yezerets, N.W. Currier, W.N. Delgass, F.H. Ribeiro, Catal. Today 136 (2008) 136.
[11] R.D. Clayton, M.P. Harold, V. Balakotaiah, Appl. Catal. B: Environ. 84 (2008) 616.
[12] A. Lindholm, N.W. Currier, J. Li, A. Yezerets, L. Olsson, J. Catal. 258 (2008) 273.
[13] L. Cumaranatunge, S.S. Mulla, A. Yezerets, N.W. Currier, W.N. Delgass, F.H. Ribeiro, J. Catal. 246 (2007) 29.
[14] L. Lietti, I. Nova, P. Forzatti, J. Catal. 257 (2008) 270.
[15] J. Günther, B. Konrad, B. Krutzsch, A. Nolte, D. Voigtländer, M. Weibel, M. Weirich, G. Wenninger, Patent US 6,338,244 B1 (2002).
[16] P. Forzatti, L. Lietti, Catal. Today (in press), doi:10.1016/j.cattod.2008.11.023.
[17] P. Kočí, M. Schejbal, J. Trdlička, T. Gregor, M. Kubíček, M. Marek, Catal. Today 119 (2007) 64.
[18] A. Güthenke, D. Chatterjee, M. Weibel, N. Waldbüßer, P. Kočí, M. Marek, M. Kubíček, Chem. Eng. Sci. 62 (2007) 5357.
[19] Monolith, Research group, http://www.vscht.cz/monolith (2009).
[20] P. Kočí, M. Kubíček, M. Marek, Ind. Eng. Chem. Res. 43 (2004) 4503.
[21] D. Kryl, P. Kočí, M. Kubíček, M. Marek, T. Maunula, M. Härkönen, Ind. Eng. Chem. Res. 44 (2005) 9524.
[22] P. Kočí, F. Štěpánek, M. Kubíček, M. Marek, Chem. Eng. Sci. 62 (2007) 5380.
[23] J. Jirát, M. Kubíček, M. Marek, Chem. Eng. Sci. 56 (2001) 1597.
[24] J.-S. Choi, W.P. Partridge, W.S. Epling, N.W. Currier, T.M. Yonushonis, Catal. Today 114 (2006) 102.
[25] T. Lesage, C. Verrier, P. Bazin, J. Saussey, M. Daturi, Phys. Chem. Chem. Phys. 5 (2003) 4435.
[26] J.P. Breen, R. Burch, C. Fontaine-Gautrelet, C. Hardacre, C. Rioche, Appl. Catal. B: Environ. 81 (2008) 150.
[27] S. Voltz, C. Morgan, D. Liederman, S. Jacob, Ind. Eng. Chem. Prod. Res. Dev. 12 (1973) 294.